Solid State Communications 354 (2022) 114897

Contents lists available at ScienceDirect

Solid State Communications

journal homepage: www.elsevier.com/locate/ssc

Effect of oxygen content on structural and optoelectronic properties of $ZnS_{1-x}O_x$ alloy in the wurtzite structure

S.A. Saoucha [a], I. Bouchama [a], Sultan Alomairy [b], M.A. Ghebouli [c,d], B. Ghebouli [e], M. Fatmi [d,*]

[a] Department of Electronic, Faculty of Technology, University of Mohamed Boudiaf, M'sila, 28000, Algeria
[b] Department of Physics, College of Science, Taif University, P.O. Box 11099, Taif, 21944, Saudi Arabia
[c] Department of Chemistry, Faculty of Technology, University of Mohamed Boudiaf, M'sila, 28000, Algeria
[d] Research Unit on Emerging Materials (RUEM), University Ferhat Abbas of Setif 1, Setif, 19000, Algeria
[e] Laboratory of Studies Surfaces and Interfaces of Solids Materials, Department of Physics, Faculty of Science, University Ferhat Abbas of Setif 1, Setif, 19000, Algeria

ARTICLE INFO

Communicated by Oguz Gulseren

Keywords:
DFT calculation
Structural properties
Band structure
mBJ-GGA
Absorption

ABSTRACT

The tunability of the physical parameters of $ZnS_{1-x}O_x$ alloy in the wurtzite phase makes this semiconductor potentially useful as an absorbent layer and antireflection coating. A deviation of the bulk modulus from Vegard's law is observed in $ZnS_{1-x}O_x$ alloy. Based on the density functional theory as implemented in the Wien2k code under the virtual crystal approximation, the lattice constant, bulk modulus and band gap have been calculated with both GGA and the modified Becke-Johnson potential (mBJ). The ternary $ZnS_{1-x}O_x$ alloy becomes more stable with the increase in the oxygen content x. The in-plane and out-of-plane imaginary components of the dielectric function attain non-zero magnitude at energy identical to the fundamental band gap value. The intense peaks in the in-plane and out-of-plane dielectric function located at 6.5 eV and 7.75 eV suggest inter band transition, and no photon emission in this material. $ZnS_{1-x}O_x$ absorbs ultraviolet light in the range 4 eV–10 eV, which validates its candidature for optical and photovoltaic devices. The refractive index is more important when photons move through the material and when bonds between atoms are covalent. The anisotropic optical parameters, the fundamental band gap range (2.7–3.7 eV) and absorption of extreme ultraviolet light make $ZnS_{1-x}O_x$ alloy as windows, lenses and absorber material.

1. Introduction

Group II-VI semiconductors have a wide direct band gap and are attractive materials with desired parameters, which cannot be obtained with Group III-V compounds. The cost of manufacturing II-VI semiconductors has recently decreased and their optoelectronic properties have become more important for certain applications. Ternary alloys consisting of the elements of subgroup IIb and of group VI are excellent infrared window materials [1]. The binary compounds ZnS and ZnO limit the $ZnS_{1-x}O_x$ alloy, which can take the zinc blende and wurtzite phases. The x is the concentration of oxygen in the considered alloy, which varies from 0 to 1 with a step of 0.125. The investigated alloy is intended for applications such as light emitting in photovoltaic applications [2]. A theoretical study on elastic and optical properties of $ZnS_{1-x}O_x$ in the zinc blende structure is carried out within the full potential linearized augmented plane wave method [3]. The $ZnS_{1-x}O_x$ ternary alloy exhibits desired optical and electronic parameters such as absorption coefficient and band gap. Therefore, this alloy can be used as absorber material in the photovolltaic field. In this work, the calculated band gap of $ZnS_{1-x}O_x$ alloy as a function of oxygen concentration is too large (2.683 eV–3.68 eV) for optimal photovoltaic efficiency. The study conducted by Joshua Schrier et al. on the heterostructure ZnO/ZnS proposes it as photovoltaic devices with organic polymer semiconductor as p-channel contact [4]. Salman Ali, synthetize the parents of this alloy ZnO, in the composite form with ZnS as nanostructure using various oxygen concentration [5]. The experimental study of the $ZnS_{1-x}O_x$ semiconductor alloy carried out by optical transmission gives the band gap at room temperature in the zinc blende structure [1,6]. In the field of optical and acoustic phonons, the investigation of $ZnS_{1-x}O_x$ alloy using resonant Raman spectroscopy, exhibits longitudinal optical modes for a low oxygen content and additional modes attributed to local vibrational modes (LVMs) [7]. A. Gueddim et al. present calculations on structural, electronic and optical properties of $ZnS_{1-x}O_x$ in the zinc blende phase [8]. In this work, we study the effect of oxygen concentration on

* Corresponding author.
E-mail address: fatmimessaoud@yahoo.fr (M. Fatmi).

https://doi.org/10.1016/j.ssc.2022.114897
Received 4 May 2022; Received in revised form 17 July 2022; Accepted 18 July 2022
Available online 1 August 2022

Table 1
X, Y, Z coordinates of atomic species.

Compounds	Atom	X	Y	Z
ZnS	Zn1	0.67	0.33	0.00
		0.33	0.67	0.50
	S	0.67	0.33	0.37
		0.33	0.67	0.88
ZnO	Zn1	0.33	0.67	0.00
		0.67	0.33	0.50
	O	0.33	0.67	0.38
		0.67	0.33	0.88
$ZnS_{0.875}O_{0.125}$	Zn1	0.17	0.33	0.00
	Zn2	0.33	0.17	0.50
		0.83	0.17	0.50
		0.33	0.67	0.50
	Zn3	0.66	0.33	0.00
		0.16	0.83	0.00
		0.66	0.83	0.00
	Zn4	0.83	0.67	0.50
	S5	0.17	0.33	0.38
	S6	0.33	0.17	0.88
		0.83	0.17	0.88
		0.33	0.67	0.89
	S7	0.67	0.33	0.38
		0.17	0.83	0.38
		0.67	0.83	0.38
	O8	0.83	0.67	0.88
$ZnS_{0.5}O_{0.5}$	Zn1	0.17	0.33	0.00
		0.33	0.17	0.50
	Zn2	0.67	0.33	0.00
		0.83	0.17	0.50
	Zn3	0.17	0.83	0.00
		0.33	0.67	0.50
	Zn4	0.67	0.83	0.00
		0.83	0.67	0.50
	S5	0.17	0.33	0.38
		0.33	0.17	0.88
	S6	0.67	0.33	0.38
		0.83	0.17	0.88
	O7	0.17	0.83	0.38
		0.33	0.67	0.88
	O8	0.67	0.83	0.38
		0.83	0.67	0.88

structural, electronic and optical properties of $ZnS_{1-x}O_x$ alloy in the wurtzite structure. $ZnS_{1-x}O_x$ is a semiconductor alloy with potential light-emitting and solar-cell applications. It has adequat absorption coefficient and band gap compared with those in zinc blende phase. The computation has been done with the full-potential linearized augmented plane wave (FP-LAPW) method in the framework of the density functional theory (DFT) as implemented in the WIEN2k computer package. It is well known that the GGA functional that are commonly used for total-energy calculations, such as PBE, provide band gaps that are much smaller than experiment. Thus, one has to resort to other methods to get reliable results for the band gap. Hybrid functionals (HSE), the GW and (TB-mBJ) approaches give values closer to the experiment [9]. The optical properties reveal a high absorption coefficient (200×10^4 cm^{-1}) in the UV region, an average reflectivity of approximately 0.5% with a high transmittance, an optical conductivity of 9000 $\Omega^{-1}cm^{-1}$. These parameters make $ZnS_{1-x}O_x$ a promising material as an absorbent layer and antireflection coating.

2. Calculation process

We carried out the calculations using the full-potential linearized augmented plane wave (FP LAPW) method as implemented in the WIEN2k computer package [10]. We apply the so-called GGA-PBESOL [11] in the structural study. We use the Tran-Blaha modified Beck-Johnson (TB-mBJ) potential [12] for treating the exchange–correlation effect in the electronic properties. The TB-mBJ has attracted a lot of interest recently because of the surprisingly accurate band gaps they can deliver for many semiconductors and insulators. But for the compound having the d or f band; the approach could not be more appropriate [13]. The test based on K-points was performed and found best convergence within 0.1 meV at 1000 K-points in the whole Brillouin zone for each concentration x, where a grid of $9 \times 9 \times 10$ was adopted. The calculations were performed on $2 \times 2 \times 1$ supercells containing 16 atoms. We expand the wave function in the interstitial sites with a k cut-off such as $k_{max} = 7.0/RMT$, where RMT is the smallest atomic sphere radius (muffin-tin radius) and k_{max} denotes the magnitude of the largest k-vector. We extend the valence wave functions inside the muffin-tin sphere and the charge density up to $l_{max} = 10$ and Gaussian's parameter was $G_{max} = 14$ (Ryd)1/2. The MT radii take the values 1.7, 1.75 and 1.8 for O, S and Zn atoms. It is not possible to perform the DFT in the presence of light in the Wien2K code.

3. Results and discussions

3.1. 1. structure and lattice parameters

The study of $ZnS_{1-x}O_x$ ternary alloy is carried out in the wurtzite structure, where, x varies in the range 0–1 with a step of 0.125. X, Y, Z coordinates of Atomic species are reported in Table 1. We utilize the full-potential linearized augmented plane wave (FP LAPW) method as implemented in the WIEN2k computer package. We obtain the accurate form factor result of the interested ternary $ZnS_{1-x}O_x$ as a function of those related to their binary compounds ZnO and ZnS.

$$W_{ZnS_{1-x}O_X}(x) = xW_{ZnO} + (1-x)W_{ZnS} \quad (1)$$

The bulk modulus of ternary $ZnS_{1-x}O_x$ alloy could be also determined in terms of those of bulk modulus of the constituents binary compounds ZnO and ZnS using Vegard's law [14].

$$B_{ZnS_{1-x}O_X}(x) = xB_{ZnO} + (1-x)B_{ZnS} \quad (2)$$

We report in Table 2 the lattice parameters a and c, bulk modulus B and its pressure derivative B' for various oxygen content x. Our results of ZnS and ZnO binary compounds are compared to their available

Table 2
The lattice parameters, bulk modulus and its pressure derivative for $ZnS_{1-x}O_x$ alloy.

	x	0	0.125	0.250	0.375	0.5	0.625	0.750	0.875	1
a (Å)	T.W.	3.2815	3.3744	3.4815	3.5463	3.6001	3.635	3.7605	3.8005	3.8487
	Oth	3.281 [16]								4.05 [15]
	Exp	3.2501 [18]								3.68 [19]
c (Å)	T.W.	5.2553	5.4041	5.5755	5.6793	5.7654	5.8214	6.0223	6.0863	6.2954
	Oth	5.256 [16]								6.14 [17]
	Exp	5.2071 [18]								6.252 [20]
B(GPa)	T.W.	127.51	115.25	102.87	93.1	85.89	80.36	75.5	73.22	69.63
	Oth	133.7 [21]								88 [22]
	Exp	142.7 [22]								80.1 [21]
B'	T.W.	4.32	4.39	4.55	4.51	4.49	4.47	4.48	4.38	4.41
	Oth	4.05 [15]								4.4 [17]
	Exp	3.6 [22]								4.41 [23]

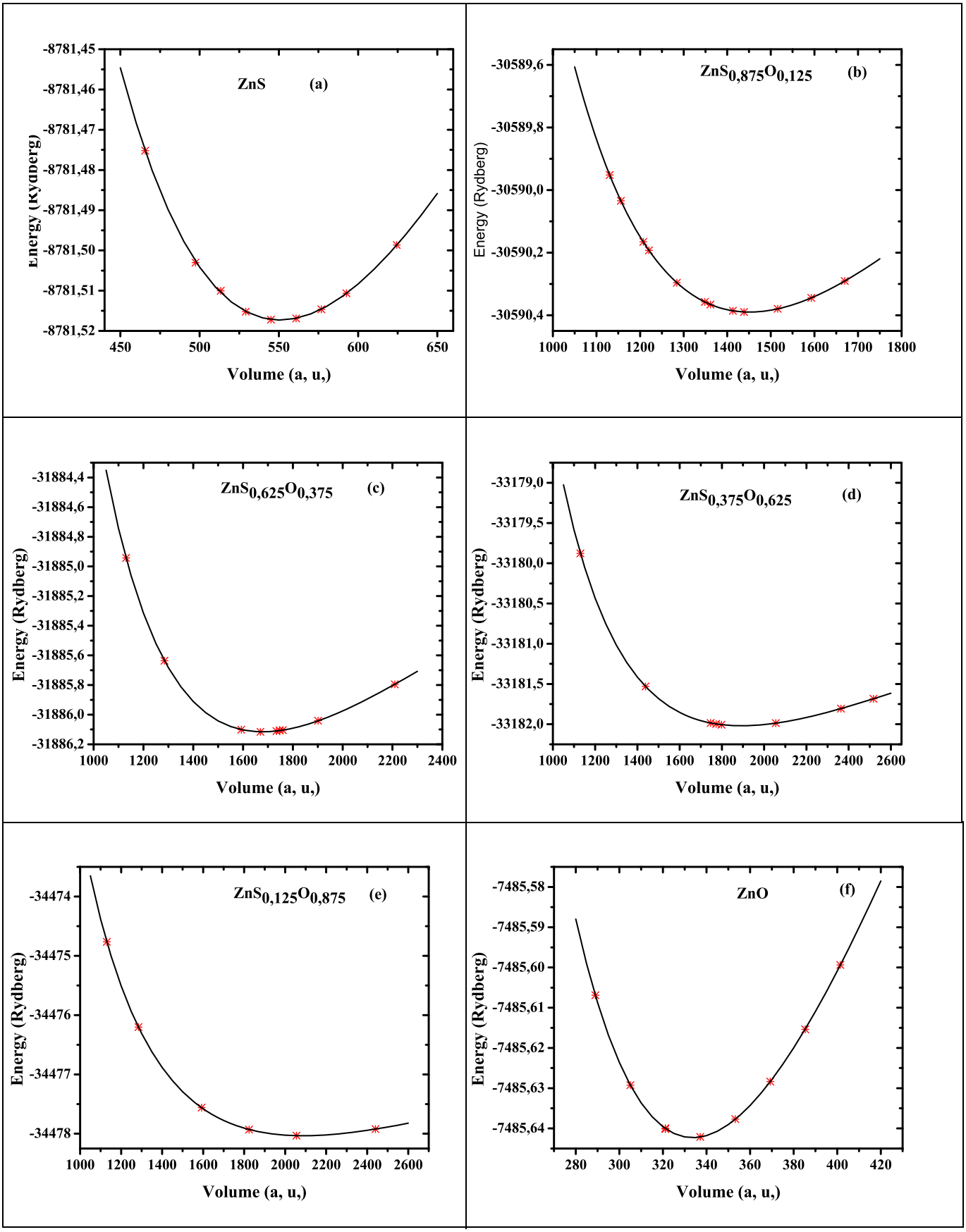

Fig. 1. The impact of unit cell volume on energy for (a) ZnS, (b) $ZnS_{0.875}O_{0.125}$, (c) $ZnS_{0.625}O_{0.375}$, (d) $ZnS_{0.375}O_{0.625}$, (e) $ZnS_{0.125}O_{0.875}$ and (f) ZnO using PBE-GGA functional.

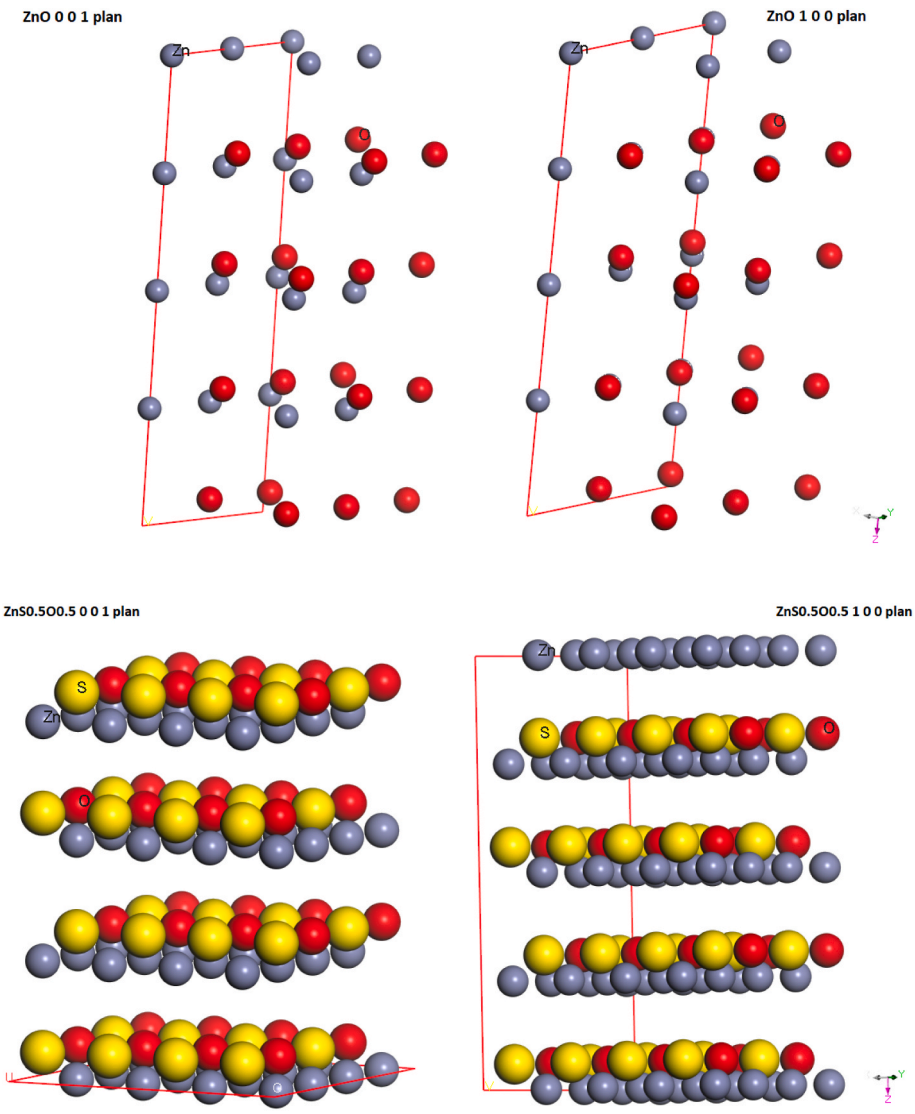

Fig. 2. The surface orientations (100) and (001) in ZnO and $ZnS_{0.5}O_{0.5}$.

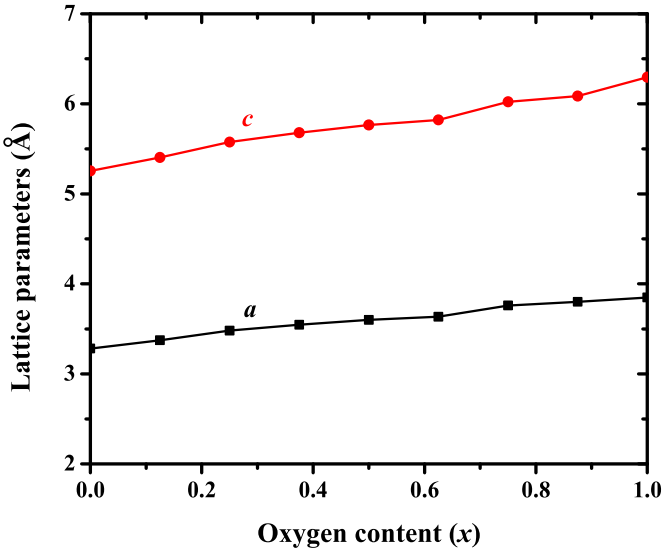

Fig. 3. The impact of oxygen content x on lattice parameters (a) and (c) according to GGA approximation for the $ZnS_{1-x}O_x$ alloy.

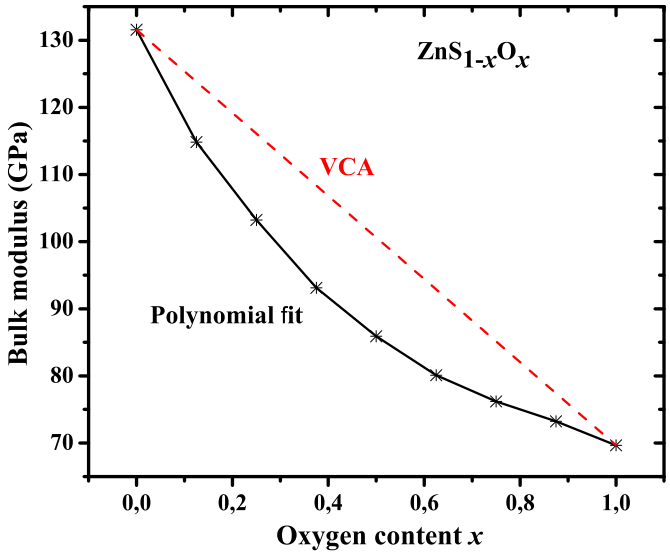

Fig. 4. The effect of oxygen content x on bulk modulus of $ZnS_{1-x}O_x$ calculated according to GGA approximation and compared with the VCA method.

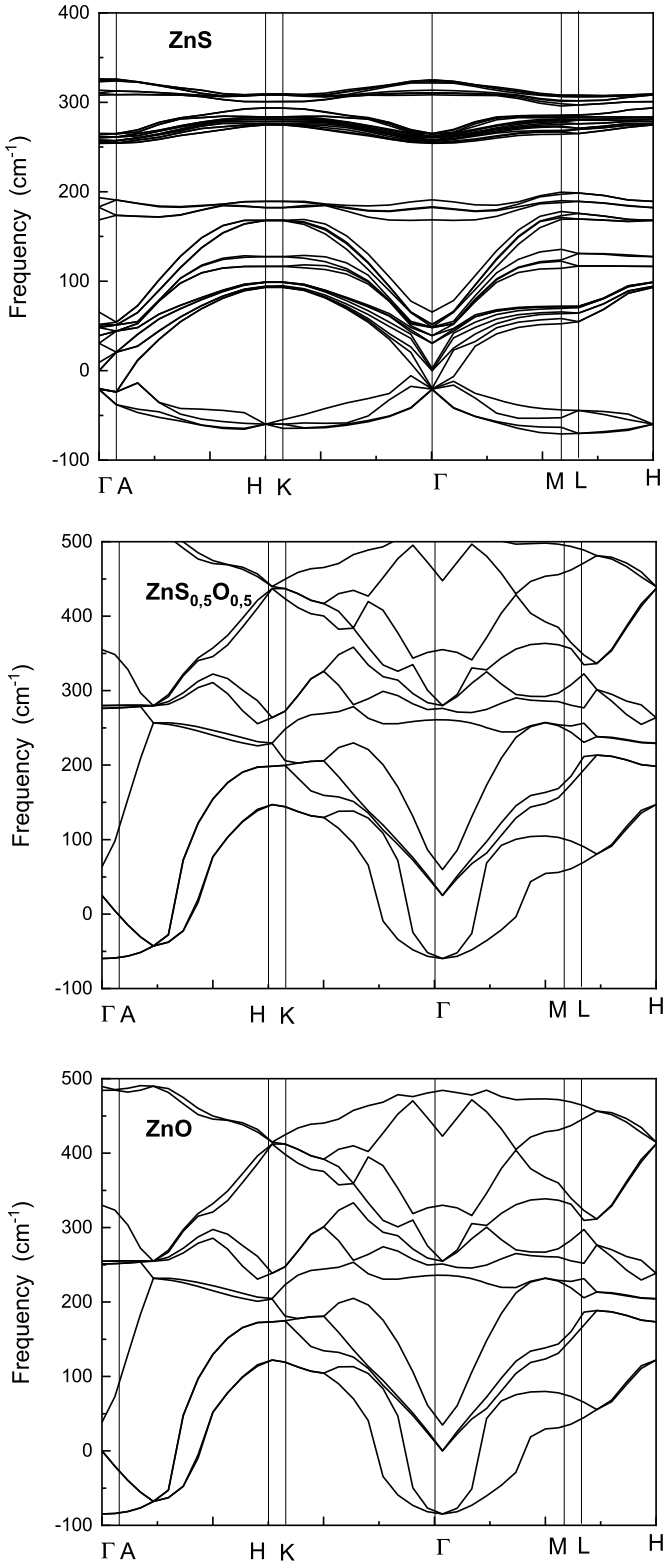

Fig. 5. The spectrum of phonons in wurtzite ZnS, $ZnS_{0.5}O_{0.5}$ and ZnO structures.

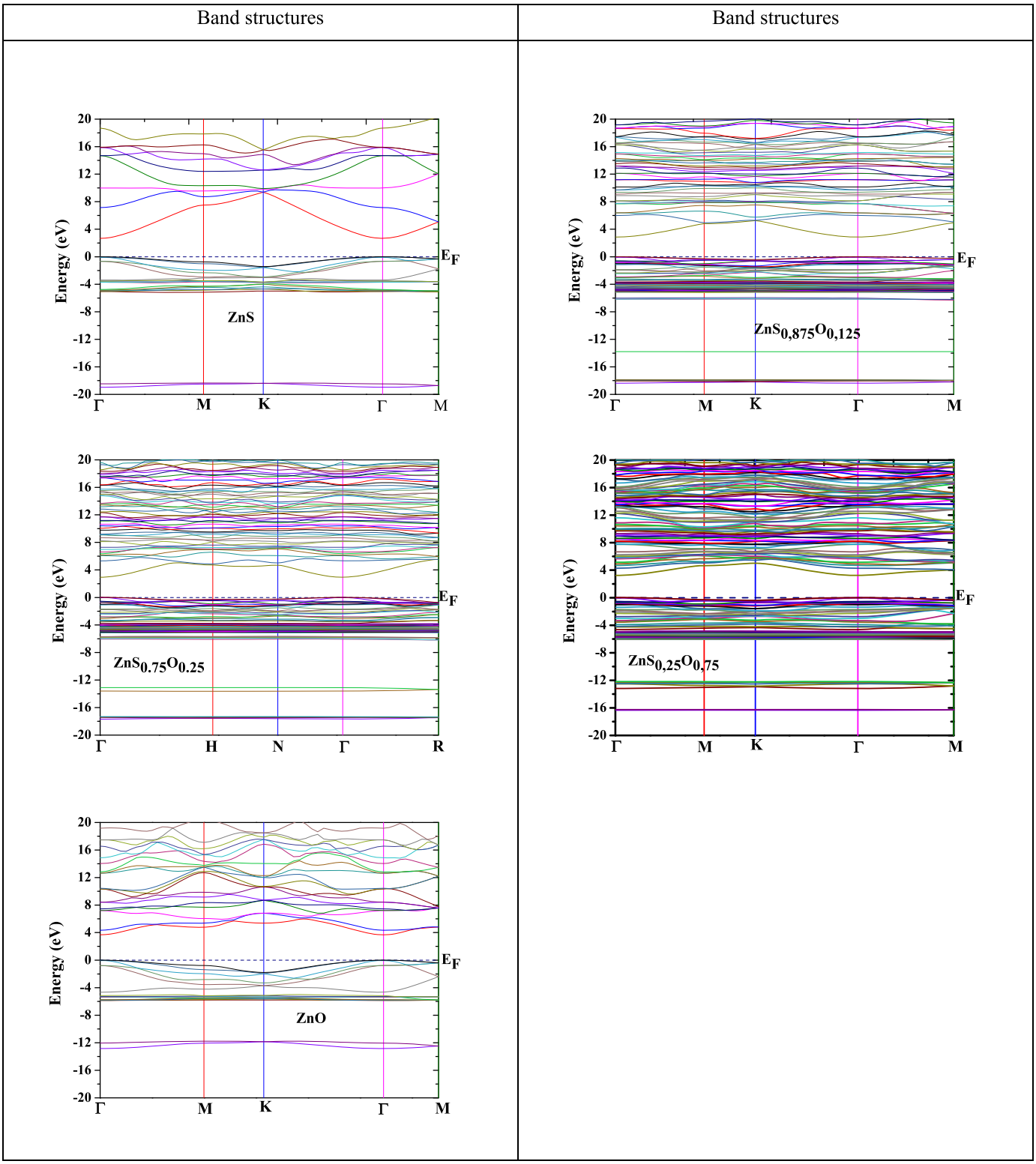

Fig. 6. Band structures of ZnS, $ZnS_{0.875}O_{0.125}$, $ZnS_{0.75}O_{0.25}$, $ZnS_{0.25}O_{0.75}$ and ZnO at high symmetry points Γ, M, K, H, N and R calculated according to GGA approximation.

Table 3
The direct Γ-Γ band gap of $ZnS_{1-x}O_x$ alloy.

	x	0	0.125	0.250	0.375	0.5	0.625	0.750	0.875	1
E_g (eV)	T.W.	2.6836	2.8622	2.9551	2.9601	3.0602	3.1377	3.2384	3.383	3.6809
	Oth	2.68 [14]	2.78 [20]	3 [19]		2.82 [19]		3.05 [19]		3.6 [19]
	Exp	3.03 [20]		2.831 [21]		2.77 [21]		3.03 [21]		3.7 [2]

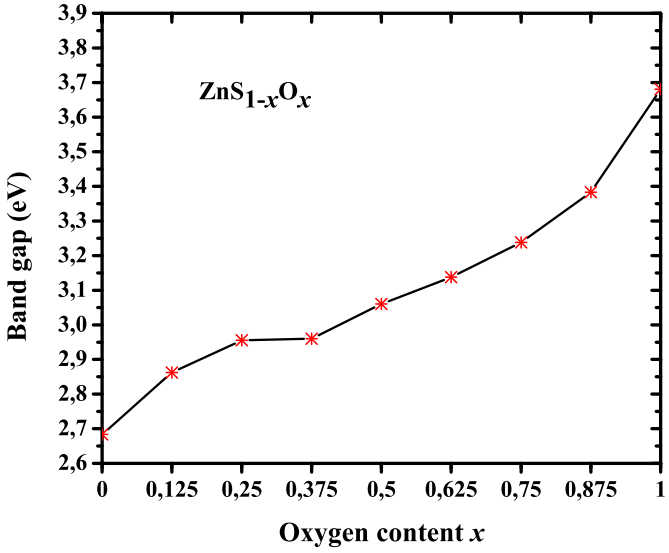

Fig. 7. Band gap as a function of oxygen content x for relaxed $ZnS_{1-x}O_x$ alloy using the mBJ-GGA.

theoretical [15–17] and experimental [18–20] data quoted in the literature, which are in good agreement. We show in Fig. 1 (a), (b), (c), (d), (e) and (f) the impact of unit cell volume on energy for ZnS, $ZnS_{0.875}O_{0.125}$, $ZnS_{0.625}O_{0.375}$, $ZnS_{0.375}O_{0.625}$, $ZnS_{0.125}O_{0.875}$ and ZnO. It is noted that the ternary alloy becomes more stable with the increase in the oxygen content x. The surface orientations (100) and (001) in ZnO and $ZnS_{0.5}O_{0.5}$ is shown in Fig. 2. We present in Fig. 3 the impact of oxygen content on the lattice parameters for $ZnS_{1-x}O_x$ ternary alloy. Both parameters a and c increase slightly when O content x increases. The second-order fit of lattices parameters a and c gives the following relations:

$$a(x) = 3.29683 + 0.6999\,x - 0.13165\,x^2 \tag{3}$$

$$c(x) = 5.296619 + 0.934504\,x + 0.046215\,x^2 \tag{4}$$

The bulk modulus and its pressure derivative calculated within GGA method are displayed in Table 2. The values for binary compounds agree reasonably with the theoretical data [15,17,21] and experimental values [21–23]. Fig. 4 shows the effect of oxygen content x on bulk modulus calculated according to GGA approximation and compared with the VCA method. It is reported that the GGA model is in good agreement with the VCA method. The spectrum of phonons in wurtzite ZnS, $ZnS_{0.5}O_{0.5}$ and ZnO as shown in Fig. 5 have a negative part, implying their dynamical instability. $ZnS_{1-x}O_x$ in wurtzite structure has adequat band gap and absorption coefficient, which allow its use as an absorber in solar cells. While zinc blende structure is more stable.

3.2. 2. Band structure and projected DOS

We will discuss the electronic band structures and the projected densities of states (PDOS) of materials. We show in Fig. 6 the band structures of $ZnS_{1-x}O_x$ alloy, where $x = 0$, 0.125, 0.25, 0.75 and 1 calculated with both GGA and the modified Becke-Johnson potential (TB-mBJ). The lowest energy of conduction band is at Γ point, while the highest energy of valence band is at Γ point, which indicate a direct Γ-Γ band gap for ZnS, $ZnS_{0.875}O_{0.125}$, $ZnS_{0.75}O_{0.25}$, $ZnS_{0.25}O_{0.75}$ and ZnO. The upper valence band is located between −4.85 eV and the Fermi level E_F. The direct Γ-Γ band gap of $ZnS_{1-x}O_x$ alloy is reported in Table 3. The corresponding band structures of ZnS, $ZnS_{0.875}O_{0.125}$, $ZnS_{0.75}O_{0.25}$, $ZnS_{0.25}O_{0.75}$ and ZnO are a semiconductor with a band gap of 2.6836 eV, 2.8622 eV, 2.9851 eV, 3.2384 eV and 3.5809 eV, which is conform to available theoretical data [14,19,20] experimental value [2,20,21]. The band gap obtained by the (TB-mBJ) approximation is closer to the experimental value comparing to that given by the GGA + U or LDA + U [24]. Tran-Blaha modified Becke-Jahnson exchange potential approximation (TB-mBJ) was used to improve the electronic properties specifically band gap value. We visualize in Fig. 7 the effect of oxygen content x on the fundamental band gap of $ZnS_{1-x}O_x$ alloy, which increases when x increases. This is in agreement with $Zn_{1-x}Mg_xO$ alloy, where the band gap increases with the Mg concentration [25]. (TB-mBJ) approach better estimates the value of the electronic band gap much closer to the value of band gap calculated experimentally [26].

The polynomial fit of order 2 gives the following relation:

$$E_g(x) = 2.76295 + 0.31954\,x + 0.51989\,x^2 \tag{5}$$

We report in Fig. 8 the projected densities of states for $ZnS_{1-x}O_x$ alloy, where $x = 0$, 0.5 and 1. The common features in the PDOS profile for the studied compounds consist in the fact that Zn d and O p have a similar profile throughout the whole energy region, indicating the presence of hybridization between Zn d and O p electrons and covalent

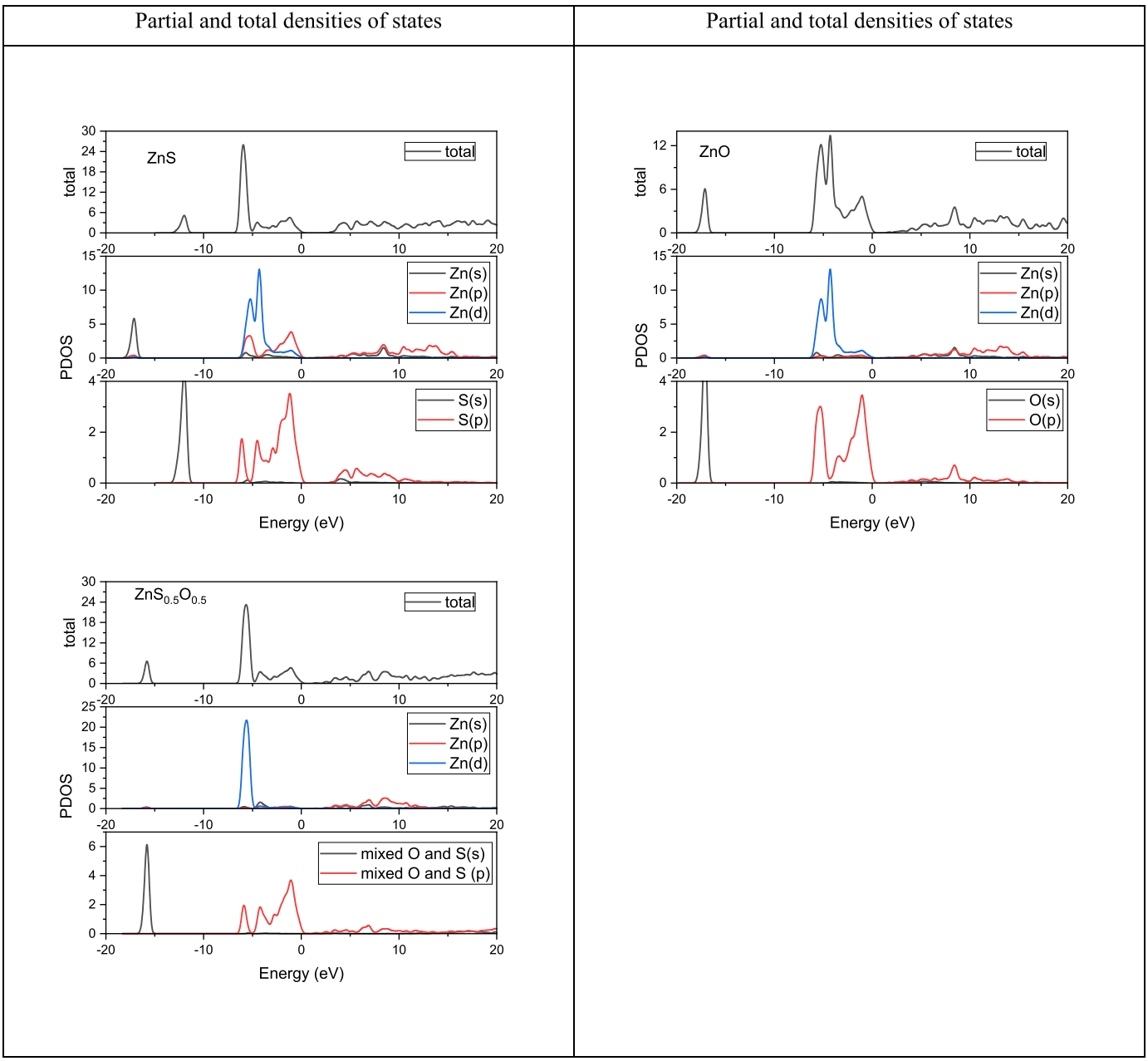

Fig. 8. Projected partial densities of states of ZnO, ZnS and $ZnS_{0.5}O_{0.5}$.

bonding between them. The contribution at the upper valence band is mainly the Zn d and O p states. The lower conduction band is empty in all compounds, so the transitions occur from O p and Zn d states. Practically the description of charges in molecules requires the distribution of the system into atomic fragments. One share the charge density at each point between atoms in proportion to the free atomic density, such that the distribution of bound and localized atoms resembles the molecular density. Atomic charges and multipole moments summarize the reorganization of molecular charges, which allows the calculation of the external electrostatic potential and the interaction energy between molecules.

Mulliken population's analysis of ZnS and ZnO compounds allows the description of charge transfer and binding interactions in molecular systems. We report in Tables 4 and 5 the lengths and overlap populations of the shortest atomic bonds, Hirshfeld, population and charges of ZnS and ZnO. We display also the partial atomic charges (Mulliken populations) in the different atoms for ZnS and ZnO. The atomic charges given by the calculations follow the expected chemical trends and are also similar to the Hirshfeld atomic charges. From Tables 4 and 5, it is seen that there is relatively large charge transfer from Zn site to O state in the inner region as compared to Zn to S atoms in the outer region. The calculated Mulliken population could explain the charge transfer and bond type after bonding. A positive value for the atomic population indicates the degree of atoms losing an electron, whereas a negative value reflects the amount of atoms gaining an electron. In addition, a bond with a larger bond population has stronger covalent characteristics. The average population values of Zn and O atoms in ZnO were 0.83 and −0.83, suggesting that Zn atoms tend to lose electrons and O atoms

Table 4
Atomic Populations (Mulliken), bond, length and Hirshfeld analysis of ZnS.

Species	Ion	s	p	d	f	Total	Charge(e)
S	1	1.82	4.67	0.00	0.00	6.49	−0.49
S	2	1.82	4.67	0.00	0.00	6.49	−0.49
Zn	1	0.58	0.95	9.98	0.00	11.51	0.49
Zn	2	0.58	0.95	9.98	0.00	11.51	0.49

Bond	Population	Length (Å)
S 2 – Zn 1	162	235721
S 1 – Zn 2	162	235721
S 1 – Zn 1	018	236066
S 2 – Zn 2	018	236066

All bands spilling parameter for spin component 1 = 2.12%.

Hirshfeld Analysis

Species	Ion	Hirshfeld	Charge (e)	Spin (hbar/2)
S	1	−0.23	0.00	
S	2	−0.23	0.00	
Zn	1	0.23	0.00	
Zn	2	0.23	0.00	

Table 5
Atomic Populations (Mulliken), bond, length and Hirshfeld analysis of ZnO.

Species	Ion	s	P	d	f	Total	Charge (e)
O	1	1.86	4.97	0.00	0.00	6.83	−0.83
O	2	1.86	4.97	0.00	0.00	6.83	−0.83
Zn	1	0.49	0.71	9.97	0.00	11.17	0.83
Zn	2	0.49	0.71	9.97	0.00	11.17	0.83

Bond	Population	Length (Å)
O 2 – Zn 1	1.11	1.99777
O 1 – Zn 2	1.11	1.99777
O 2 – Zn 2	0.20	2.00612
O 1 – Zn 1	0.20	2.00612

All bands spilling parameter for spin component 1 = 0.85%.

Hirshfeld Analysis

Species	Ion	Hirshfeld	Charge (e)	Spin (hbar/2)
O	1	−0.34	0.00	
O	2	−0.34	0.00	
Zn	1	0.34	0.00	
Zn	2	0.34	0.00	

tend to gain electrons. While, the average population of Zn and S atoms in ZnS were 0.49 and −0.49, suggesting that Zn atoms tend to lose electrons and S atoms tend to gain electrons. The calculated Zn1–O2 and Zn2–O1 (Zn1–S2 and Zn2–S1) population and bond length are 0.20 and 2.00612 Å (1.62 and 2.35721 Å). The computed Zn1–S1 and Zn2–S2 (Zn1–O1 and Zn2–O2) population and bond length are 0.18 and 2.36066 Å (0.20 and 2.00612 Å).

3.3. 3. Optical properties

The real and imaginary part of the dielectric function, the absorption coefficient, the optical conductivity, the refractive index and extinction coefficient, the reflectivity and the electrons energy loss were calculated for in-plane [100] and out-of-plane [001] crystallographic directions in the optimized wurtzite structure. These parameters are anisotropic for a material in the wurtzite phase. We report in Fig. 9 the effect of photon energy on the real part of the dielectric function for in-plane [100] and out-of-plane [001] directions, where the static dielectric function value is in the range 2.3–4.3 when x content varies from 0 to 1. The real dielectric function helps in predicting the nonlinear optical behavior of the material. Fig. 10 visualizes the impact of photon energy on the imaginary part of the dielectric function for in-plane [100] and out-of-plane [001] crystallographic directions for $ZnS_{1-x}O_x$ alloy at various oxygen content x. The imaginary part of the dielectric function

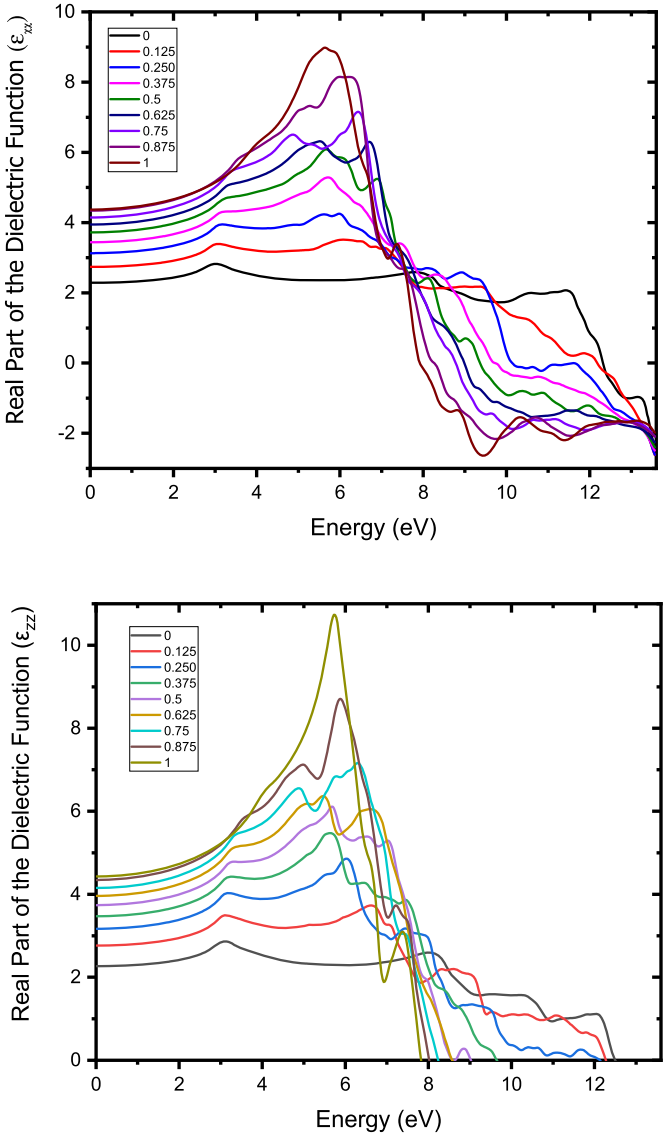

Fig. 9. The effect of photon energy on (a) in-plane and (b) out-of-plane real part of the dielectric function for $ZnS_{1-x}O_x$ alloy at various oxygen content x.

represents the absorptive capacity of such material. We can observe that the in-plane and out-of-plane imaginary components of the dielectric function attain non-zero magnitude at energy identical of that corresponding to the direct Γ-Γ band gap value of $ZnS_{1-x}O_x$ alloy. The intense peaks in the in-plane and out-of-plane dielectric function are located at 6.5 eV, 7.75 eV, which suggest inter band transition, and the photon emission is not possible in this material. The peak intensity in both real and imaginary parts of the dielectric function increases when the oxygen content decreases. We represent in Fig. 11 the absorption coefficient as a function of photon energy when the incidence is in-plane [100] and out-of-plane [001] crystallographic directions for $ZnS_{1-x}O_x$ alloy at various oxygen content x. The absorption coefficient is directly connected to the extinction coefficient by:

$$\alpha(\omega) = \frac{2\omega}{C}k \tag{6}$$

This material is reported to absorb ultraviolet light in the range 4 eV–10 eV. This improvement validates the candidature of $ZnS_{1-x}O_x$ material for optical and photovoltaic devices. It is pointed out that the absorption coefficient of $ZnS_{1-x}O_x$ system is in the range of 10^5 cm^{-1}, which is a characteristic property of a good absorber material. We show

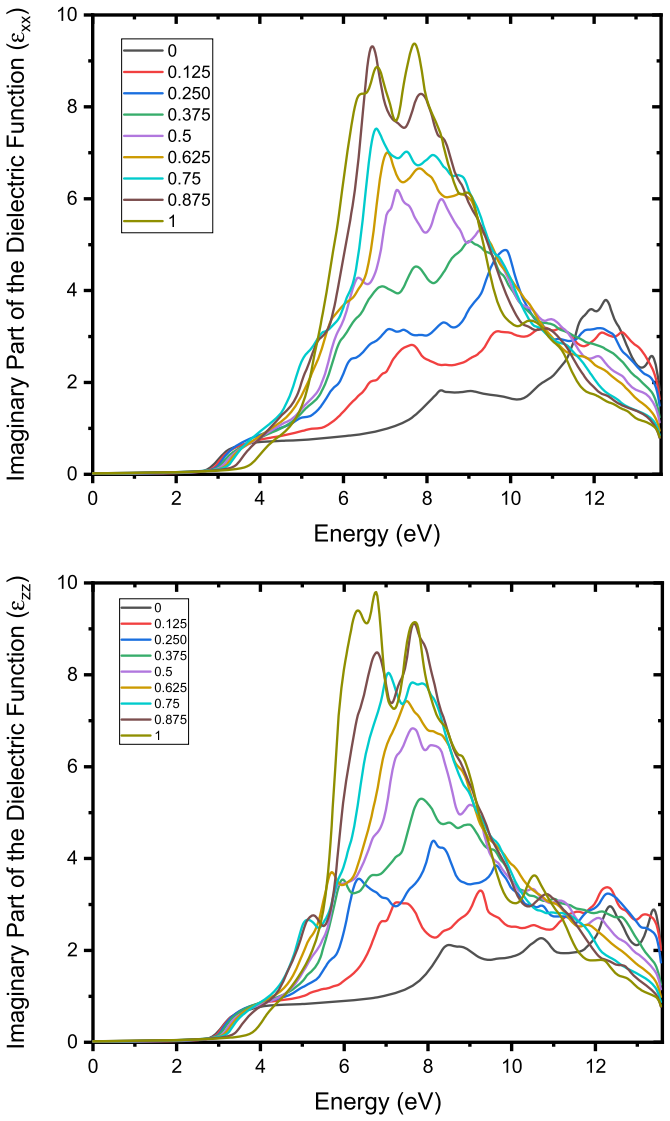

Fig. 10. The effect of photon energy on (a) in-plane and (b) out-of-plane imaginary. Part of the dielectric function for $ZnS_{1-x}O_x$ alloy at various oxygen content x.

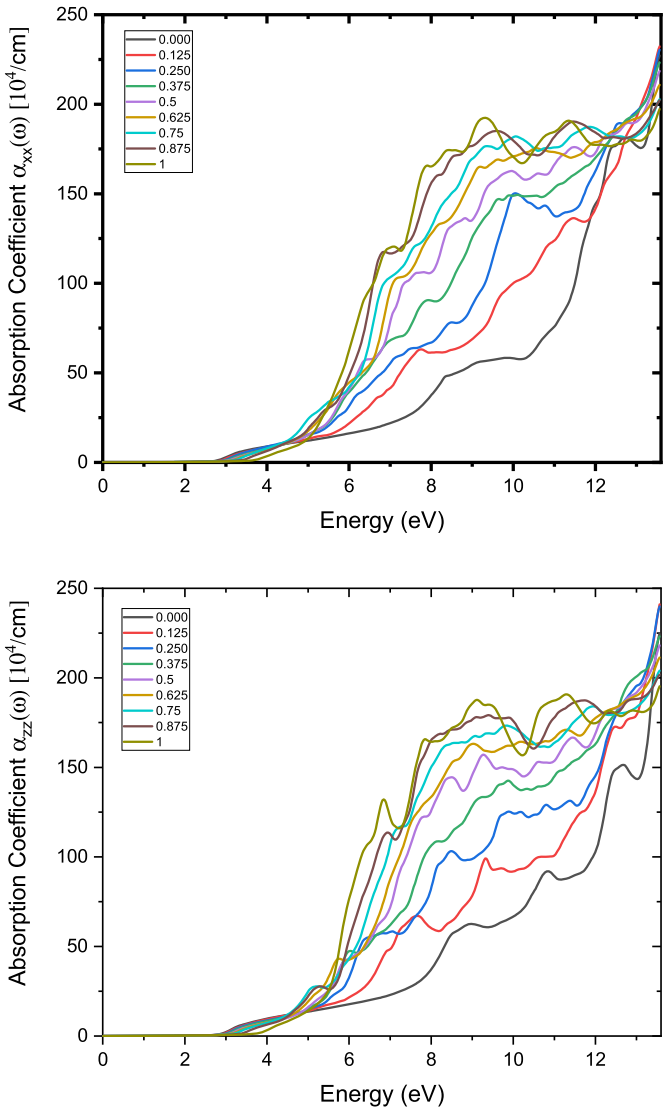

Fig. 11. The effect of photon energy on (a) in-plane and (b) out-of-plane absorption coefficient of $ZnS_{1-x}O_x$ alloy at various oxygen content x.

in Fig. 12 the effect of photon energy on optical conductivity with incidence along in-plane [100] and out-of-plane [001] crystallographic directions of $ZnS_{1-x}O_x$ alloy at various oxygen content x. The optical conductivity is connected to imaginary part of the dielectric function.

$$\sigma(\omega) = \frac{\omega}{4\pi}\varepsilon_2(\omega) \tag{7}$$

For the spectral range from 3.5 eV to 12.5 eV the out-of-plane component of the optical conductivity is identical to the respective in-plane counterpart. The flat in the conductivity spectrum is estimated to be 9000 $\Omega^{-1}cm^{-1}$ and positioned between 6 eV and 8 eV. The optical conductivity increases with increasing oxygen content x. The complex refractive index N is defined as: $N = n + ik$, where $n(\omega)$ is the refractive index and $k(\omega)$ is the extinction coefficient. The complex refractive index N is directly related to the dielectric constant $N = \sqrt{\varepsilon}$, refractive index and extinction coefficient are directly associated with the following expressions:

$$n(\omega) = \frac{\sqrt{\varepsilon_1^2(\omega) + \varepsilon_2^2(\omega)} + \sqrt{\varepsilon_1(\omega)}}{\sqrt{2}} \tag{8}$$

$$\kappa(\omega) = \frac{\sqrt{\varepsilon_1^2(\omega) + \varepsilon_2^2(\omega)} - \sqrt{\varepsilon_1(\omega)}}{\sqrt{2}} \tag{9}$$

We plot in Fig. 13 the effect of photon energy on the refractive index and the extinction coefficient for in-plane [100] and out-of-plane [001] crystallographic directions of $ZnS_{1-x}O_x$ alloy at various oxygen content x. The refractive index of the material measures its transparency to incident spectral radiation. The static refractive index increases from 1.5 to 2.1 as the oxygen content x passes from 0 to 1. The in-plane and out-of-plane extinction coefficient starts at energy identical of that corresponding to the direct band gap value of $ZnS_{1-x}O_x$ alloy. The refractive index is more important when photons move through the material and when bonds between atoms are covalent. Fig. 14 reports the effect of photon energy on in-plane and out-of-plane reflectivity of $ZnS_{1-x}O_x$ alloy at various oxygen content x. The reflectivity is a measure of the ability of

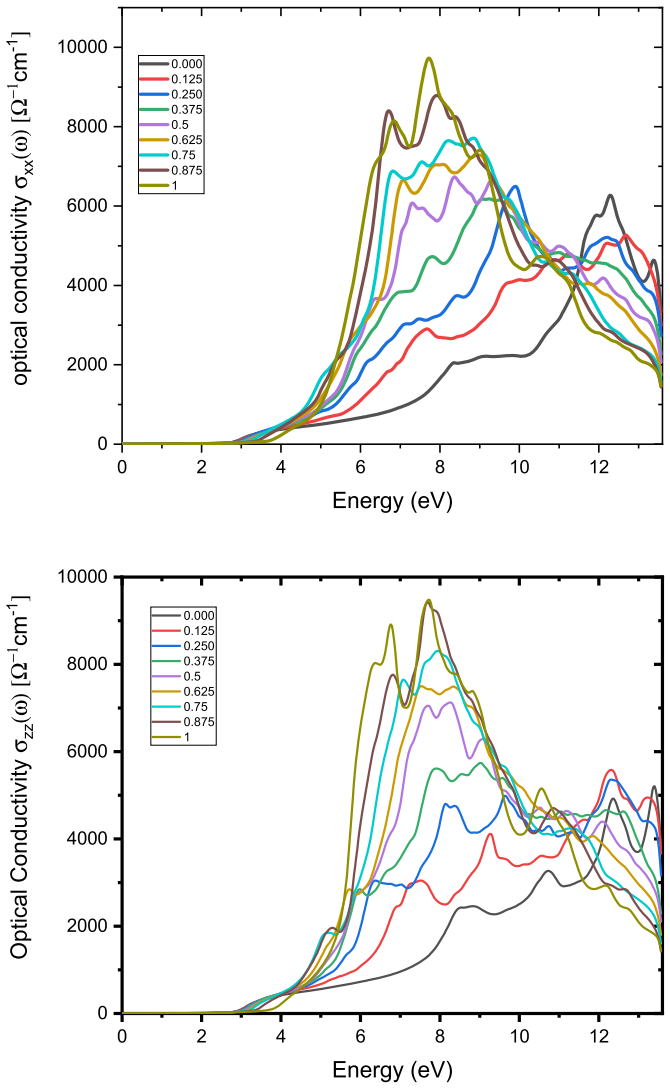

Fig. 12. The effect of photon energy on (a) in-plane and (b) out-of-plane optical conductivity of $ZnS_{1-x}O_x$ alloy at various oxygen content *x*.

a material to reflect radiation. The reflectivity is given as a function of refractive index and extinction coefficient by;

$$R(\omega) = \frac{(n-1)^2 + \kappa^2}{(n+1)^2 + \kappa^2} \tag{10}$$

The reflectivity of $ZnS_{1-x}O_x$ alloy starts at photon energy around 3 eV and reaches several peaks of maxima and minima in the field of extreme ultraviolet light. In practice, the roughness, uniformity of thickness, inter diffusion, oxidation and thermal stability limit the reflectivity. The anisotropic optical parameters, the band gap range (2.5–3.6 eV) and absorption of extreme ultraviolet light make $ZnS_{1-x}O_x$ alloy as windows, lenses and absorber material. Fig. 15 gives the effect of photon energy on in-plane and out-of-plane electron energy loss of $ZnS_{1-x}O_x$ alloy at various oxygen content *x*. The electron energy loss is related to real and imaginary parts of dielectric function.

$$L(\omega) = \frac{\varepsilon_2(\omega)}{[\varepsilon_1^2(\omega) + \varepsilon_2^2(\omega)]} \tag{11}$$

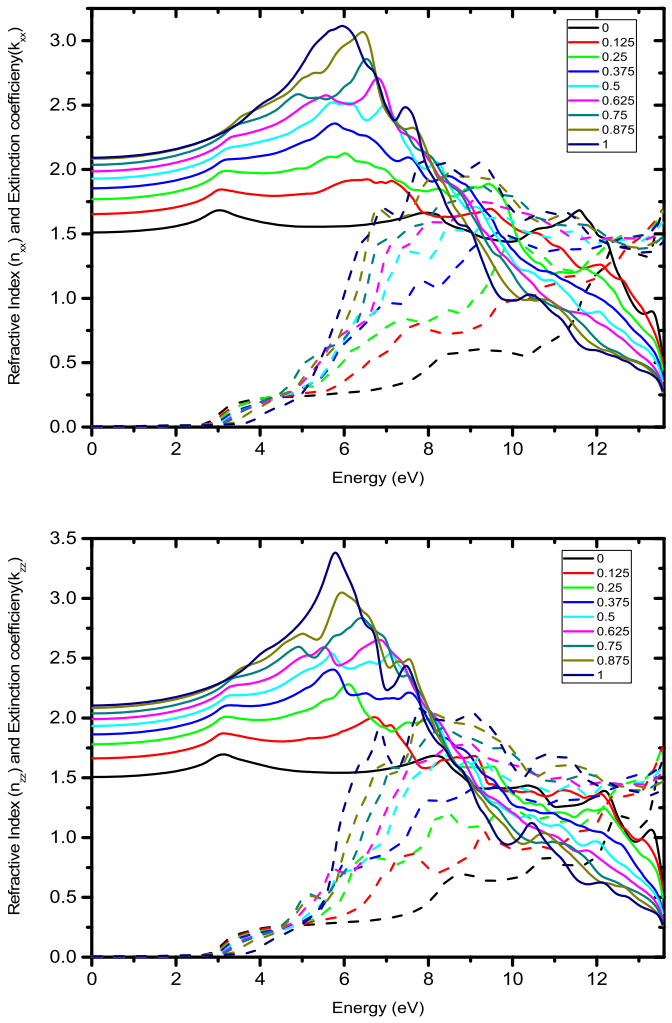

Fig. 13. The effect of photon energy on (a) in-plane and (b) out-of-plane refractive index and extinction coefficient of $ZnS_{1-x}O_x$ alloy at various oxygen content *x*.

The features of the energy-loss spectra are related to the photonic band structure of the crystal. The interaction of the electron with the crystal contributes to the energy loss. The electron energy loss of $ZnS_{1-x}O_x$ alloy is localized in the extreme ultraviolet light region.

4. Conclusion

This study used the DFT method to investigate the structure and optoelectronic properties of $ZnS_{1-x}O_x$ system. The anisotropic optical parameters, the band gap range from 2.5 eV to 3.6 eV and absorption of extreme ultraviolet light make $ZnS_{1-x}O_x$ alloy as windows, lenses and absorber material. The refractive index is more important when photons move through the material and when bonds between atoms are covalent. The static refractive index increases from 1.5 to 2.1 when the oxygen content *x* passes from 0 to 1. The in-plane and out-of-plane extinction coefficient start at energy identical of that corresponding to the direct band gap value of $ZnS_{1-x}O_x$ alloy. $ZnS_{1-x}O_x$ absorb ultraviolet light in the range 4 eV–10 eV and the band gap validate its candidature for optical and photovoltaic devices. The similar profile of Zn d and O p throughout the whole energy region indicates the presence of hybridization between

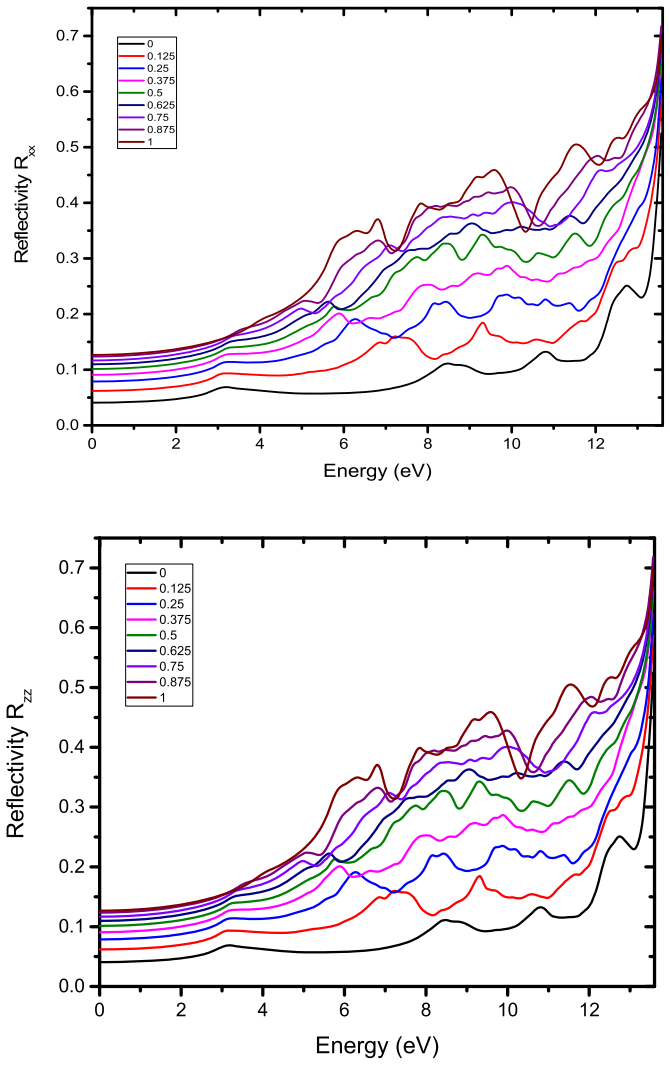

Fig. 14. The effect of photon energy on (a) in-plane and (b) out-of-plane reflectivity of $ZnS_{1-x}O_x$ alloy at various oxygen content *x*.

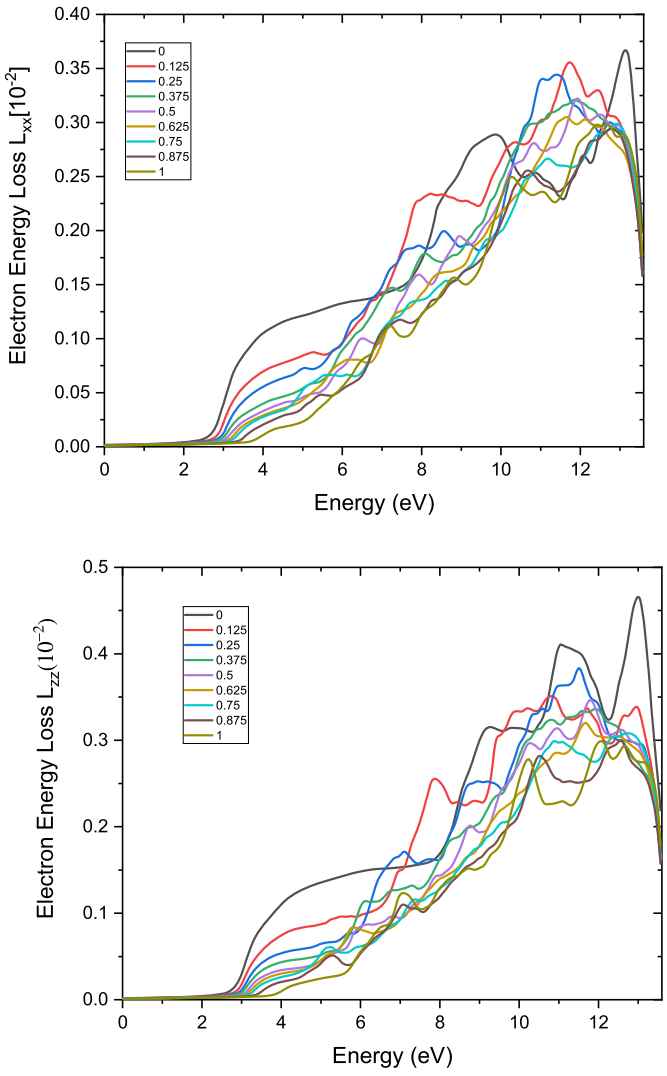

Fig. 15. The effect of photon energy on (a) in-plane and (b) out-of-plane electron energy loss of $ZnS_{1-x}O_x$ alloy at various oxygen content *x*.

their electrons and a covalent bonding between them. The absorption coefficient of $ZnS_{1-x}O_x$ system is in the range of 10^5 cm^{-1}, which is a characteristic property of a good absorber material.

Author statement

Saoucha: Project administration, Resources, Software, Supervision. Bouchama: Investigation. Alomairy: Validation. M. Ghebouli: Data curation. **B. Ghebouli**: Writing - review editing. Fatmi: Conceptualization, Formal analysis, Funding acquisition, Methodology, Visualization, Writing – original draft.

Declaration of competing interest

The authors declare that they have no known competing financial interests or personal relationships that could have appeared to influence the work reported in this paper.

Data availability

The authors do not have permission to share data.

Acknowledgements

We would like to thank Taif University Research Supporting Project number (TURSP-2020/63), Taif University, Taif, Saudi Arabia.

References

[1] Junfu QiXi'an, Yuefeng YinMonash, Xiangdong Ding, Jun Sun, Junkai Deng, Mater. Today Commun. 5 (2020) 101259. DOI :10.1016/J.MTCOMM.2020.101259.
[2] Jesse Huso, Leah Bergman, Matthew D. McCluskey, J. Appl. Phys. 125 (2019), 075704, https://doi.org/10.1063/1.5064371.
[3] A. Bellouche, Ahmed Gueddim, S. Zerroug, Nadir Bouarissa, Optik - Int. J. Light Electron Optics 127 (23) (2016) 11374–11378. DOI:10.1016/j.ijleo.2016.09.034.
[4] Joshua Schrier, Denis O. Demchenko, , Lin-Wang, A. Paul Alivisatos, Nano Lett. 7 (8) (2007) 2377–2382, https://doi.org/10.1021/nl071027k.
[5] Salman Ali, Sumaiya Saleem, Muhammad Salman, Majid Khan, Mater. Chem. Phys. 248 (2020) 122900.
[6] J. Huso, L. Bergman, M. McCluskey, Mater. Sci., J. Appl. Phys. 125 (2019), 075704, https://doi.org/10.1063/1.5064371.
[7] Jesse Huso, Jacob R. Ritter, Dinesh Thapa, Kin Man Yu, Leah Bergman, Matthew D. McCluskey, J. Appl. Phys. 123 (2018), 161537, https://doi.org/10.1063/1.4998748.
[8] A. Gueddim, S. Zerroug, N. Bouarissa, Phil. Mag. 95 (24) (2015) 2627–2638.
[9] Peter Blaha, Karlheinz Schwarz, Fabien Tran, Robert Laskowski, Georg K. H. Madsen, Laurence D. Marks, J. Chem. Phys. 152 (2020), 074101, https://doi.org/10.1063/1.5143061.
[10] P. Blaha, K. Schwarz, G. Madsen, D. Kvasnicka, J. Luitz, WIEN2k, an Augmented Plane Wave+Local Orbitals Program for Calculating Crystal Properties, Karlheinz Schwarz, Techn. Universität Wien, Austria, 2001.

[11] J.P. Perdew, A. Ruzsinszky, G.I. Csonka, O.A. Vydrov, G.E. Scuseria, L. A. Constantin, X. Zhou, K. Burke, Phys. Rev. Lett. 100 (13) (2008) 136406.
[12] F. Tran, P. Blaha, Phys. Rev. Lett. 102 (22) (2009), 226401, https://doi.org/10.1103/PhysRevLett.102.226401.
[13] H. Zaari, A.G. El hachimi, A. Benyoussef, A. El Kenz: Journal of Magnetism and Magnetic Materials, https://doi.org/10.1016/j.jmmm.2015.05.032.
[14] L. Vegard, Z. Phys. 5 (1921) 17.
[15] J.E. Jaffe, J.A. Snyder, Z. Lin, A.C. Hess, Phys. Rev. B Condens. Matter 62 (2000) 1660–1665.
[16] A.S. Mohammadi, S.M. Baizaee, H. Salehi, World Appl. Sci. J. 14 (2011) 1530–1536.
[17] H. Rozale, L. Beldi, B. Bouhafs, P. Ruterana, Phys. Status Solidi (B) Basic Res. 244 (2007) 1560–1566.
[18] E.H. Kisi, M.M. Elcombe, Acta Crystallogr. Sect. C Cryst. Struct. Commun. 45 (1989) 1867–1870.
[19] R. Chowdhury, S. Adhikari, P. Rees, Phys. B Condens. Matter 405 (2010) 4763–4767.
[20] S. Desgreniers, L. Beaulieu, I. Lepage, Phys. Rev. B Condens. Matter 61 (2000) 8726–8733.
[21] K. Kihara, G. Donnay, Can. Mineral. 23 (1985) 647–654.
[22] S. Desgreniers, Phys. Rev. B Condens. Matter 58 (1998) 14102–14105.
[23] E. Chang, G.R. Barsch, J. Phys. Chem. Solid. 34 (1973) 1543–1563.
[24] Adil Es-Smairi, Nejma Fazouan, El Houssine Atmani, E. Maskar, Tuan V. Vu, D. P. Rai, Int. J. Quant. Chem. (2021). DOI:10,22541/au.161907539.90276790/v1.
[25] Fayyaz Hussain, Muhammad Imran, R.M. Arif Khalil, Niaz Ahmad Niaz, Anwar Manzoor Rana, M. Atif Sattar, Muhammad Ismail, Abdul Majid, Sungjun Kim, Faisal Iqbal, M. Arshad Javid, Sadaf Saeed, Abdul Sattar, Phys. E Low-dimens. Syst. Nanostruct. 115 (2020) 113658.
[26] Ejaz Ahmad Khera, Hafeez Ullah, Muhammad Imran, N.A. Niaz, Fayyaz Hussain, R. M. Arif Khalil, Umbreen Rasheed, M. Atif Sattar, Fasial Iqbal, Chandreswar Mahta, Anwar Manzoor Rana, Sungjun Kim, Optik - Int. J. Light Electron Optics 212 (2020) 164677.

Update

Solid State Communications

Volume 356, Issue , 15 November 2022, Page

DOI: https://doi.org/10.1016/j.ssc.2022.114967

Solid State Communications 356 (2022) 114967

Contents lists available at ScienceDirect

Solid State Communications

journal homepage: www.elsevier.com/locate/ssc

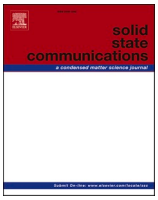

Corrigendum

Corrigendum to "Effect of oxygen content on structural and optoelectronic properties of $ZnS_{1-x}O_x$ alloy in the wurtzite structure" [Solid State Commun. 354 (2022) 114897]

S. Ali Saoucha [a], I. Bouchama [a], Sultan Alomairy [b], M.A. Ghebouli [c,d], B. Ghebouli [e], M. Fatmi [d,*]

[a] Department of Electronic, Faculty of Technology, University of Mohamed Boudiaf, M'sila, 28000, Algeria
[b] Department of Physics, College of Science, Taif University, P.O. Box 11099, Taif, 21944, Saudi Arabia
[c] Department of Chemistry, Faculty of Technology, University of Mohamed Boudiaf, M'sila, 28000, Algeria
[d] Research Unit on Emerging Materials (RUEM), University Ferhat Abbas of Setif 1, Setif, 19000, Algeria
[e] Laboratory of Studies Surfaces and Interfaces of Solids Materials, Department of Physics, Faculty of Science, University Ferhat Abbas of Setif 1, Setif, 19000, Algeria

The authors regret **S. Ali-Saoucha[a], I. Bouchama[a], S. Alomairy[b], M.A. Ghebouli[c,d], B. Ghebouli[e], M. Fatmi[d]**.

The authors would like to apologise for any inconvenience caused.

DOI of original article: https://doi.org/10.1016/j.ssc.2022.114897.
* Corresponding author.
E-mail address: fatmimessaoud@yahoo.fr (M. Fatmi).

https://doi.org/10.1016/j.ssc.2022.114967

Available online 29 September 2022